Modeling Carbon Dioxide Vibrational Frequencies in Ionic Liquids: II. Spectroscopic Map

Clyde A. Daly Jr.,[1] Eric J. Berquist,[2,3] Thomas Brinzer,[2,3] Sean Garrett-Roe,[2,3] Daniel S. Lambrecht,[2,3] and Steven A. Corcelli[1]

[1] Department of Chemistry and Biochemistry, University of Notre Dame, 251 Nieuwland Science Hall, Notre Dame, Indiana 46656

[2] Department of Chemistry, University of Pittsburgh, 219 Parkman Ave., Pittsburgh, Pennsylvania 15260

[3] Pittsburgh Quantum Institute, University of Pittsburgh, 3943 O'Hara St., Pittsburgh, Pennsylvania 15260

Abstract

The primary challenge for connecting molecular dynamics (MD) simulations to linear and two-dimensional infrared (2D-IR) measurements is the calculation of the vibrational frequency for the chromophore of interest. Computing the vibrational frequency at each time step of the simulation with a quantum mechanical method like density functional theory (DFT) is generally prohibitively expensive. One approach to circumnavigate this problem is the use of spectroscopic maps. Spectroscopic maps are empirical relationships that correlate the frequency of interest to properties of the surrounding solvent that are readily accessible in the MD simulation. Here, we develop a spectroscopic map for the asymmetric stretch of CO_2 in the 1-butyl-3-methylimidazolium hexafluorophosphate ($[C_4C_1im][PF_6]$) ionic liquid (IL). DFT is used to compute the vibrational frequency of 500 statistically independent CO_2-$[C_4C_1im][PF_6]$ clusters extracted from an MD simulation. When the map was tested on a 500 different CO_2-$[C_4C_1im][PF_6]$ clusters, the correlation coefficient between the benchmark frequencies and the predicted frequencies was $R = 0.94$ and the root mean squared error was 2.7 cm^{-1}. The calculated distribution of frequencies also agrees well with experiment. The spectroscopic map required information about the CO_2 angle, the electrostatics of the surrounding solvent, and the Lennard-Jones interaction between the CO_2 and the IL. The contribution of each term in the map was investigated with symmetry-adapted perturbation theory (SAPT) calculations.

I. Introduction

Ionic liquids (ILs) have attracted tremendous attention because of their properties as environmentally friendly alternatives to volatile organic solvents, and their applications involving the production, storage, and efficient utilization of energy.[1–5] ILs exhibit unique physical properties relative to conventional liquids in terms of vapor pressure, viscosity, electrical and thermal conductivity, solubility of polar and nonpolar molecules, and melting point.[5–9] Moreover, these properties can be tuned to specific applications by chemically modifying the molecules that comprise the liquid. For example, by functionalizing the molecules of an IL to react with CO_2, improved design for preferentially separating CO_2 from gas mixtures was achieved.[9–13] Thus, ILs offer a promising new direction for the removal of environmentally harmful CO_2 from postcombustion flue gas.

It is essential that the fundamental structure and dynamics of ILs be understood to aid in the design of new ILs for unique applications. Unlike conventional solvents, ILs exhibit heterogeneous structure and dynamics that have profound implications for their physical properties. Two-dimensional infrared (2D-IR) spectroscopy offers several unique advantages for interrogating the structure and dynamics of liquids because of its exquisite time and spatial resolution.[14–17] The spatial resolution results from the size of suitably chosen vibrational chromophores. The vibrational frequencies of these reporters depend sensitively on their local environment.[15,18–22] As that local environment evolves, so too will the vibrational frequency of the probe – a process called spectral diffusion. 2D-IR spectroscopy measures these frequency fluctuation dynamics, which relate back to the intrinsic dynamics of the surroundings of the vibrational chromophore.

Recently, Brinzer *et al*. have demonstrated that the asymmetric stretch of CO_2 (ν_3) is an excellent vibrational reporter of its local environment in ILs.[23] In particular, these experiments have established (1) that the asymmetric stretch of CO_2 exhibits a significant solvatochromic shift with respect to the choice of anion in a series of imidazolium-based ILs, (2) that the CO_2 vibrational population lifetime is sufficiently long to measure 2D-IR spectra on a 100 ps timescale, and (3) that the longest spectral diffusion timescale correlates empirically with the viscosity of the IL.[23] Fayer and coworkers have also studied CO_2 in ILs with 2D-IR spectroscopy, including detailed measurements and modeling of the rotational dynamics of CO_2 and how this motion results in reorientational-induced spectral diffusion (RISD). Through analysis of polarization-selective 2D-IR measurements, the RISD contribution to the overall spectral diffusion process was quantified.[24,25] The RISD analysis assumed that shifts in the CO_2 vibrational frequency were governed by a second-order Stark effect.

Among multidimensional vibrational spectroscopy's great successes was revealing the dynamics of hydrogen-bond network rearrangements in liquid water.[26–39] However, these profound insights were only possible in conjunction with a robust theoretical effort.[21,29–31,40–59] Much of that theoretical effort focused on the development and application of empirical relationships connecting the instantaneous vibrational frequency of interest to structural properties – usually the electrostatics – of the surrounding condensed-phase environment.[22,41,60] Such relationships have come to be known as "spectroscopic maps." With a spectroscopic map in hand, quantities such as the linear IR absorption spectrum, 2D-IR spectra, and the frequency fluctuation correlation function that quantifies spectral diffusion, can be readily calculated in a conventional molecular dynamics (MD) simulation.[47,60,61] With the emergence of 2D-IR

measurements on CO_2 in ILs, there is ample motivation to develop a spectroscopic map for the asymmetric stretch of CO_2 in an IL.

In paper I, we developed and validated a robust quantum mechanics/molecular mechanics (QM/MM) protocol for calculating anharmonic CO_2 vibrational frequencies in the 1-butyl-3-methylimidazolium hexafluorophosphate ([C_4C_1im][PF_6]) IL. Here, we have used the protocol to calculate the asymmetric stretch vibrational frequency of CO_2 in 1000 statistically independent snapshots extracted from an MD simulation. For each frequency calculation, the CO_2 molecule and two pairs of IL molecules are treated quantum mechanically with density functional theory (DFT). The rest of the solvent is included in the calculation as point charges that polarize the quantum mechanical region. The two-dimensional potential energy surface for the CO_2 stretches is constructed on a 12×12 grid and the resulting vibrational Schrödinger equation is solved using a discrete variable representation (DVR) method. Once the vibrational frequencies were calculated, 500 of these snapshots were used to parameterize the spectroscopic map and the other 500 snapshots were used to quantify the accuracy of the spectroscopic map.

Previous spectroscopic maps have primarily been based on electrostatics,[19,42,62–66] but our initial quantum chemistry investigations[23,67] indicate that the antisymmetric stretch of CO_2 is sensitive to other physical effects, including charge transfer, dispersion, exchange repulsion, and electrostatics. Accordingly, we found that a suitably accurate spectroscopic map could not be constructed using only electrostatic properties of the IL environment. Instead, we had to include both electrostatic and Lennard-Jones (LJ) terms in the map. Błasiak and Cho previously found that including dispersion interactions resulted in an improved spectroscopic map for the amide I vibration of *N*-methylacetamide.[68] In addition, since the CO_2 molecule was modeled as flexible

in solution, the map also has a dependence on the CO_2 bend angle whose contribution was investigated in detail.

Spectroscopic maps are inherently empirical and can, in principle, utilize any variable that is sufficiently correlated with the vibrational frequencies, even if that variable is not the cause of the vibrational frequency shifts. Therefore, the dual goals of this work are to develop and validate a spectroscopic map, and to understand how the causal variables manifest themselves in the map. To achieve the first goal, the average frequency and distribution of vibrational frequencies were compared to inhomogeneous vibrational spectra extracted from 2D-IR measurements. To achieve the second goal a selection of snapshots were analyzed with symmetry adapted perturbation theory (SAPT)[69–71] calculations.

In addition to the intermolecular interactions, CO_2 has an important intramolecular degree of freedom, the bending mode. Our previous work[23] has implicated the bending mode in the experimentally observed solvatochromic shifts. At room temperature, the bending mode has an energy of approximately $3k_BT$, placing it in an intermediate regime where it is not clear if a flexible (classical) or a rigid (quantum) model should be more appropriate. To better understand the role of CO_2 flexibility in the spectroscopic map, we calculated histograms of vibrational frequencies for a rigid (bond angle = 180°) and a flexible model of CO_2 in the [C_4C_1im][PF_6] IL. We also examined a third possibility where the CO_2 is modeled as flexible in the MD simulation, but the bend angle is relaxed prior to applying the spectroscopic map.

The paper is organized as follows. In Section II the details of the MD simulations and the anharmonic vibrational frequency calculations are described. In Section III, the spectroscopic map is constructed. In Section IV, the spectroscopic map is validated by comparison to experiment. In Section V, the contributions of the electrostatic, exchange repulsion, and

dispersive interactions in the spectroscopic map are analyzed with ALMO and SAPT calculations. Finally, in Section VI we provide some concluding remarks.

II. Computational Methods

Molecular dynamics (MD) simulations were performed using the large-scale atomic/molecular massively parallel simulator (LAMMPS)[72] with a time step of 2 fs. 256 ion pairs of $[C_4C_1im][PF_6]$ and one molecule of CO_2 were simulated at 300 K in a cubic box with periodic boundary conditions. Previous studies have confirmed that 256 ion pairs is a sufficiently large simulation box to mitigate finite-size effects.[73] The original atomic coordinates and box size (45 Å) were generated from a previous study of $[C_4C_1im][PF_6]$ containing a single water solute, which had been subjected to a rigorous equilibration protocol.[61] The water was replaced with a CO_2 solute, and was subjected to the following equilibration procedure: (1) 1 ns in the NVT ensemble at 300 K, (2) heating to 600 K over 1 ns, (3) cooling to 300 K over 1 ns, (4) 1 ns in the NVT ensemble at 300 K, and (5) 1 ns in the NVE ensemble. Production run trajectories were collected in the NVE ensemble. Energy conservation was excellent, with fits to the energy and temperature over 10 ns revealing slopes of 3.3×10^{-5} kcal mol^{-1} ps^{-1} and 9.8×10^{-6} K ps^{-1}, respectively. All molecules were modeled as fully flexible except for bonds containing hydrogen, which were held fixed at their equilibrium lengths using the SHAKE algorithm.[74,75] Also, in certain cases (see below), the CO_2 bond lengths and angle were held fixed at their equilibrium values using the LAMMPS rigid integrator.[72] The force fields for $[C_4C_1im][PF_6]$ were the same as in our previous simulation studies involving this IL.[61] Briefly, the bends, bonds, dihedrals, and Lennard-Jones parameters for $[C_4C_1im]^+$ are from the generalized Amber force field (GAFF),[76,77]

and partial charges were obtained from DFT calculations.[78] The $[PF_6]^-$ force field parameters were from the work of Liu *et al.*[79] Charges on the ions were scaled by 0.84 to empirically account for charge transfer and polarization effects in the IL.[80,81] CO_2 was modeled using the TraPPE force field, with additional terms developed by Perez-Blanco and Maginn for flexible bond lengths and angle.[82,83] Lennard-Jones interactions were truncated at 15 Å and the long-ranged electrostatics were computed using particle-mesh Ewald summation with a 15 Å real space cutoff.[84]

In order to create a spectroscopic map, 1000 statistically independent snapshots separated by 50 ps were collected from a pair of 50 ns simulations, one with a fully flexible CO_2 and a second with a fully rigid CO_2. For each snapshot, the Born-Oppenheimer potential energy surface (PES) for CO_2 stretching modes was obtained from single point energy calculations performed as the CO bond lengths were stretched from 0.955 Å to 1.45 Å in 0.045 Å steps. During these calculations, the nearest two pairs of ions by center of mass were included quantum mechanically, and the remaining ions within 20 Å were included as their point charges from the MD force field. The resulting PES was included in a discretized construction of the Hamiltonian for CO stretches, which was then diagonalized, producing the asymmetric stretch frequency. More details about this method can be found in paper 1 of this series. Least squares multiple linear regression was used to empirically fit the electric field due to the anions and cations along the CO bonds and the Lennard-Jones potential energy on the CO_2 carbon and oxygens to the asymmetric stretch of CO_2 for 500 of the flexible snapshots, and the accuracy of the resulting fit was tested using the remaining 500 snapshots. 500 of the rigid snapshots were used as a secondary test set. This is described in more detail in section IV. In certain cases, the CO_2 angle from the flexible simulation was relaxed holding all other degrees-of-freedom and the CO_2

center of mass fixed prior to vibrational frequency calculations for further analysis. This is discussed further in Section V.B.

III. Spectroscopic Map for CO_2 Vibrations

Empirical spectroscopic maps relate the instantaneous vibrational frequency of an IR reporter to properties of its surroundings that can be readily accessed in MD simulations.[47,61,85] Once a spectroscopic map has been parameterized, it can be used to calculate IR absorption spectra, 2D-IR spectra, and frequency fluctuation time correlation functions from a MD simulation. For the asymmetric stretch of CO_2 in $[C_4C_1im][PF_6]$, we were unable to obtain a suitably accurate spectroscopic map from electrostatics alone. Instead, we needed to include information about the CO_2 bend angle, as well as the Lennard-Jones (LJ) interactions between CO_2 and the surrounding IL. The spectroscopic map has the following form

$$\omega_a = \omega_g + \Delta\omega_\theta + \Delta\omega_{solvent}$$

(1)

where ω_a is the predicted CO_2 asymmetric stretch vibrational frequency, ω_g is the experimental gas phase frequency (2349.1 cm^{-1}), $\Delta\omega_\theta$ is the dependence of the frequency on the OCO bend angle, and $\Delta\omega_{solvent}$ captures the change in the vibrational frequency due to interactions with the IL solvent. Figure 3 shows the dependence of the CO_2 asymmetric stretch vibrational frequency on the OCO angle, θ, calculated for CO_2 isolated in the gas-phase. The calculated data are fit exquisitely well ($R^2 = 0.999$) by the single-parameter function

9

$$\Delta\omega_\theta = a(1 + \cos\theta)$$

<div align="right">(2)</div>

where $a = -1160.9 \text{ cm}^{-1}$.

Figure 3 also shows the vibrational frequency of 500 statistically independent $CO_2/[C_4C_1im][PF_6]$ snapshots. The vibrational frequencies were calculated using the DVR approach described in paper 1 in this series. In these calculations, the CO_2 and the closest two pairs of $[C_4C_1im][PF_6]$ molecules – determined using the distance between the center-of-mass of the IL molecule and the CO_2 carbon atom – were treated quantum mechanically at the B3LYP/6-311++G(d,p) level of theory. Any IL molecule whose center-of-mass was within 20 Å was modeled using its molecular mechanics partial atomic charges, which then polarize the quantum mechanical region. IL molecules were added to the molecular mechanics region in pairs to maintain charge neutrality. The overall trend in the vibrational frequencies roughly follows the angle dependence in the gas phase, but there is significant scatter due to interactions with the IL.

A map for the solvent effects on the asymmetric CO_2 vibrational frequency was constructed assuming the following form,

$$\Delta\omega_\text{solvent} = b_1 E_0^{Cation} + b_2 E_0^{Anion} + c_1 U_O + c_2 U_C$$

<div align="right">(3)</div>

where E and U represent contributions from the electric field and Lennard-Jones (LJ) interactions with the solvent, respectively. The subscript, C or O, indicates whether the interaction is computed at the location of the CO_2 central carbon or at the oxygen atoms. For E_O and U_O, the value used in Eq. (3) is the average for the two CO_2 oxygen sites. The LJ interaction is computed using the expression,

$$U = \sum_j \varepsilon_j \left[\left(\frac{\sigma_j}{r_j} \right)^{12} - \left(\frac{\sigma_j}{r_j} \right)^{6} \right]$$

(4)

where the sum is over all atoms in the surrounding liquid, ε_j and σ_j are the LJ parameters for the atom, and r_j is the distance to the atom. The electric fields are calculated with respect to the oxygen atoms of CO_2 and are projected along the relevant CO bond,

$$E = \hat{r}_{CO} \cdot \sum_j \frac{q_j \hat{r}_j}{r_j^2}$$

(5)

where the sum is over all relevant atoms in in the surrounding liquid (i.e. those associated with the cations for E_0^{Cation} and those associated with the anions for E_0^{Anion}), q_j is the partial atomic charge, r_j is the distance to the charge, $\hat{r}_j$ is a unit-vector directed toward the site of the charge, and $\hat{r}_{CO}$ is a unit vector from the carbon atom of CO_2 to the relevant oxygen atom. Long range electrostatics are corrected using the damped shifted force method.[86]

The four parameters, b_1, b_2, c_1, and c_2, in Eq. (3) were determined empirically by applying multiple linear regression using the 500 calculated frequencies in the training set (Table 1). The quality of the fit was evaluated using the 500 different frequencies contained in the test set (Figure 2). The root-mean-square (RMS) deviation between the test set frequencies and those predicted by Eq. (3) was 2.7 cm^{-1}, and the value of correlation coefficient for the fit was R = 0.94. By both metrics, the quality of the spectroscopic map for predicting the CO_2 asymmetric stretch vibrational frequencies in the [C$_4$C$_1$IM][PF$_6$] IL is as good or better than previously

published maps for other vibrational reporters in conventional solvents. Additionally, when 500 rigid CO_2 snapshots are used as the test set, the same level of accuracy is obtained.

The Condon approximation, that the magnitude of the transition dipole moment is independent of the vibrational frequency of a mode, fails for some solutes that interact in a strong local way with their environment. The most important example is the OH stretch of liquid water. The hydrogen bonds in water polarize the OH bond, increasing the oscillator strength on the red side of the vibrational band, which has a significant effect on the IR absorption line shape.[63,64,87] Similar to the hydrogen bonding of water, the strong local interactions of CO_2 with the ionic liquid anion could, in principle, cause the Condon approximation to fail. However, we find that the Condon approximation for the main band is adequate (Figure 3). We calculated the transition dipole moment integral, μ_{01}, of the asymmetric stretch of CO_2 in 1000 CO_2-[C$_4$C$_1$im][PF$_6$] clusters. The details of the transition dipole moment integral calculations are provided in the Supporting Information (SI). A plot of μ_{01} scaled by μ_{01}^{g}, the transition dipole moment integral of the asymmetric stretch of CO_2 in the gas-phase, versus the asymmetric stretch vibrational frequency, ω_{a}, has a slope close to zero. This confirms that it is reasonable to regard the transition dipole as a constant factor that scales the intensity of linear and non-linear spectra but does not modify their shapes. As a result, we do not treat the environmental dependence of the transition dipole moment in our spectroscopic map; we need only treat the vibrational frequencies.

IV. Physical Interpretation of the Spectroscopic Map

The average contribution to the CO_2 asymmetric stretch vibrational frequency from each of the map components is listed in Table 2. This data demonstrates that the Lennard-Jones potential energy is an important predictor of the vibrational frequency of CO_2 solvated in $[C_4C_1im][PF_6]$, while the electrostatic potential plays a secondary role. This contrasts many prior spectroscopic maps where solvatochromic frequency shifts were based purely on the electrostatics of the environment.[47,62,88] This finding is perhaps surprising at first, because one might expect electrostatics to dominate the interactions of a solute with charged solvent molecules; however, one has to consider that (1) CO_2 is not dipolar or charged, and as such will not interact with uniform electric fields very strongly, and (2) the ionic liquid, particularly the $[C_4C_1im]$ butyl tails, have large domains where the dominant interactions are dispersive. These points make it conceivable that van der Waals effects dominate the CO_2-IL interaction.

To further unravel the origin of the impact of CO_2-IL interactions on the vibrational signature of CO_2, we use the fact that the LJ contributions to the spectroscopic map can be further decomposed. In particular, we separate the LJ term into its repulsive $(\sim r^{-12})$ and attractive $(\sim r^{-6})$ contributions (Table 2). We find that the attractive and repulsive LJ terms contribute –7.0 cm^{-1} and +4.9 cm^{-1}, respectively, to the overall LJ vibrational shift of –2.1 cm^{-1}. The large contribution from the repulsive LJ term is yet another surprise. To aid in identifying the physical origins of the large repulsive LJ contribution, we performed symmetry adapted perturbation theory (SAPT)[71] calculations that decompose the total interaction energy into physically meaningful components. This analysis should be contrasted with the empirical spectroscopic map, where a good fit implies correlation but not necessarily causation. Our SAPT

calculations yield energy contributions, but it should nevertheless be possible to estimate the relative importance of different interactions for vibrational frequencies. The SAPT decomposition supports the previous discussion in that electrostatic interactions (electrostatics, induction) plus the exchange (exchange repulsion, exchange-induction) roughly cancel (total -1.3 kcal/mol at the 6-31G** DCBS level), whereas dispersive interactions dominate the interaction (total –4.7 kcal/mol from dispersion plus exchange-dispersion). However, the SAPT data also reveals that exchange-dispersion (the repulsive dispersion part) is over an order of magnitude smaller than the attractive dispersion contribution (10.1% of the total dispersion interaction). This result has to be contrasted with the ~40% contribution that the repulsive LJ potential makes to the vibrations. Since the repulsive LJ contribution is the dominant repulsive interaction incorporated in our model, the SAPT results suggest that the repulsive part of the LJ potential fits an agglomerate of exchange (Pauli) repulsion stemming from charge overlap (74.~~7~~3% of the repulsive interactions), exchange induction (2~~0.7~~1.0%) plus exchange dispersion (4.~~6~~7%).

It is likely that LJ components will be an important component of a spectroscopic map for any neutral and nonpolar solute, or any solvent where dispersive interactions, quantum effects (Pauli exchange, for instance), or higher order electrostatic interactions are particularly important. In our case, it seems logical that a higher potential at the carbon would increase the optimal length of the CO bonds, thus decreasing the local mode and normal mode frequencies. Meanwhile, at the oxygen, a larger potential would generally shorten the bond, increasing the frequency. A similar finding was observed by Brinzer et al.[23] However, these components only allow the CO_2 vibration to respond to local effects – the electric field components allow it to respond to longer-range interactions. As in prior works for different solvents and solutes, the coefficients for the two electric field components are different from each other, in this case by a

substantial margin. It has been previously established that CO_2 interacts with the anions more strongly than with the cations in an ionic liquid.[13,89–93] This is reflected in the magnitude of the coefficients related to the two components, and in their average frequency contribution (Tables 1 and 2). In particular, CO_2 is a Lewis acid and should generally interact with negatively charged moieties differently from positively charged ones.

V. Validation

A. Experimental Frequency Distribution

In order to compare our calculated distributions of CO_2 vibrational frequencies with experiment, we must account for the effects that broaden or narrow the IR absorption line shape beyond the underlying distribution of frequencies. The finite population lifetime of the asymmetric stretch vibration, reorientation of the CO_2 molecule, and a variety of other effects can broaden the absorption spectrum. On the other hand, fast dynamics can narrow the absorption spectrum (i.e. motional narrowing). A faithful comparison to experiment requires a deconvolution of these contributions to estimate the range of instantaneous frequencies experienced by CO_2.

2D-IR spectra contain sufficient information to recover the distribution of frequencies, which would be difficult to extract from the linear IR absorption spectrum alone.[23] Within the Kubo multi-exponential ansatz, the width of the frequency distribution is determined by the frequency fluctuation correlation function

$$\langle \delta\omega(t)\delta\omega(0) \rangle = \sum_{i}^{N} \Delta_i^2 \exp\left(-\frac{t}{\tau_i}\right)$$

(6)

where Δ_i^2 are the variances of frequency modulations, and τ_i are the timescales for the respective frequency fluctuations. The width of the frequency distribution is the sum of squares of the different broadening processes

$$\langle \delta\omega^2 \rangle = \sum_{i}^{N} \Delta_i^2$$

(7)

The contribution of homogeneous processes whose frequency fluctuations are too fast to be resolved (specifically when $\Delta_i\tau_i \ll 1$) can be approximated as $\delta(t)\Delta_H^2\tau_H$, which results in a frequency correlation function:

$$\langle \delta\omega(t)\delta\omega(0) \rangle = \delta(t)\Delta_H^2\tau_H + \sum_{i}^{N-1} \Delta_i^2 \exp\left(-\frac{t}{\tau_i}\right) = \frac{\delta(t)}{T_2^*} + \sum_{i}^{N-1} \Delta_i^2 \exp\left(-\frac{t}{\tau_i}\right)$$

(8)

where $T_2^* \equiv (\Delta_H^2\tau_H)^{-1}$ is the pure dephasing time and $\delta(t)$ is the Dirac delta function. The pure dephasing time depends on the variance of the fast frequency fluctuations, Δ_H^2, and the correlation time for fast motions, τ_H, and the two parameters cannot be independently determined. Analyzing the change in shape of the 2D-IR spectra as a function of the waiting time can directly determine the magnitude of frequency modulations related to the sum of exponential decays, $\sum_{i}^{N-1}\Delta_i^2$, in Eq. (8). For CO_2 in $[C_4C_1im][PF_6]$ this sum is approximately 2 cm^{-1}.[23]

Determining the magnitude of frequency modulations that give rise to the first term in Eq. (8) is more complicated. The pure dephasing time (T_2^*) is only one contributor to the experimentally determined dephasing time (T_2), which also depends on the population (T_1), and reorientational (T_{or}) motions of the molecule

$$\frac{1}{T_2} = \frac{1}{T_2^*} + \frac{1}{2T_1} + \frac{1}{3T_{or}}$$

(9)

The experimental dephasing time, T_2, of the asymmetric stretch of CO_2 in the [C$_4$C$_1$im][PF$_6$] IL is 3.3 ps.[23] Since the experiment was performed in an all-parallel polarization, we cannot unambiguously determine the population and orientation relaxation times. We can estimate them, however, based on the rate of signal decay and the orientational correlation functions determined in a similar ionic liquid.[24,25] Estimates of $T_1 = 20$ ps and $T_{or} = 10$ ps, suggest that vast majority contribution to T_2 for CO_2 in [C$_4$C$_1$im][PF$_6$] comes from pure dephasing. Population relaxation and orientational relaxation have a minor effect on the total dephasing time. We estimate a pure dephasing time of $T_2^* = 4$ ps.

Finally, the variance of the frequency fluctuations, Δ_H^2, can be limited to a range by physical constraints on the values of τ_H. The lower limit on τ_H is governed by the inertial motions of CO_2 and its ionic liquid solvent shells. The timescale of the inertial response in liquid water is in the sub-60 fs range, while that of acetonitrile is 70 fs.[29,94,95] Using 70 fs as a lower limit for τ_H places an upper limit on Δ_H of 9.7 cm^{-1}. Fits to analytical response functions suggests that $\Delta_H \tau_H \approx 0.2$ is a reasonable estimate of the dynamics that can be resolved using global fitting of the experimental data, which gives an upper limit on τ_H of 200 fs, with a corresponding lower limit on Δ_H of 6 cm^{-1}. Our estimate for the homogeneous width is thus, $6 <$

$\Delta_H < 10$ cm^{-1}. Combining the broadening due to fast and slow motions, the experimentally estimated total frequency width for CO_2 in [C$_4$C$_1$im][PF$_6$] is between 6.3 and 10.2 cm^{-1} (Figure 4).

B. Calculated Frequency Distributions

Figure 5a shows the distribution of CO_2 asymmetric stretch vibrational frequencies computed using the spectroscopic map for 1000 statistically independent snapshots collected from an MD simulation of flexible CO_2 in [C$_4$C$_1$im][PF$_6$]. These are the same snapshots that were used to parametrize and validate the spectroscopic map in Section III. The distribution is peaked at approximately 2344 cm^{-1} and its standard deviation is 7.4 cm^{-1}. Both of these values are in reasonable agreement with experiment (2342.5 cm^{-1} and 6.3 – 10.2 cm^{-1}). Qualitatively, the distribution exhibits a significant asymmetry with a mean frequency of 2339.9 cm^{-1} that is about 4 cm^{-1} to the red of the peak frequency. The experimental IR absorption line shape, however, does not show signs of such asymmetry in the underlying distribution of frequencies.

The source of the asymmetry in the distribution of frequencies in Figure 5a is the contribution to the spectroscopic map from the CO_2 bend angle, Eq. (2). This is illustrated in Figure 5c, where we have calculated the distribution of CO_2 asymmetric stretch vibrational frequencies for 1000 statistically independent snapshots collected from an MD simulation of rigid CO_2 in [C$_4$C$_1$im][PF$_6$]. Since the CO_2 molecule has an angle of 180º in each of the snapshots, the contribution to the calculated vibrational frequency from the CO_2 bend angle is zero. The resulting distribution is correctly symmetric with a mean frequency of 2346.5 cm^{-1} and a standard deviation of 2.3 cm^{-1}. The calculated distribution is centered 4 cm^{-1} to the blue of the

18

experimental distribution, and it is narrower than the lower estimate of the experimental distribution by 4 cm^{-1}.

The results in Figure 5a and 5c represent two extremes – one where the CO_2 bend is treated classically (Figure 5a) and another where the CO_2 bend is effectively neglected (Figure 5c). When the CO_2 bend is classical, it is assumed that the CO_2 asymmetric stretch vibrational frequency depends on the instantaneous value of the bend angle, Figure 1 and Eq. (2). However, the asymmetric distribution suggests that this approach is incorrect. In fact, a simple thought experiment reinforces the problems associated with regarding the CO_2 bend as a classical variable. Consider a non-rotating CO_2 molecule isolated in the gas-phase. If all of the vibrations of the CO_2 molecule are quantum mechanical, the distribution of each of the four vibrations is a delta function. However, if the bend is classical with a kinetic energy commensurate with room temperature, the distribution of asymmetric stretch vibrational frequencies will incorrectly have a finite width. One solution to this conundrum is to adopt a fully quantum mechanical treatment of the CO_2 vibrations. This would require the construction of a four-dimensional potential energy surface for each of the 1000 benchmark CO_2-[C$_4$C$_1$im][PF$_6$] clusters, which is computationally intractable.

An alternate strategy is to treat the influence of the CO_2 bend on the asymmetric stretch vibrational frequency using first-order perturbation theory. Instead of utilizing the instantaneous CO_2 angle in Eq. (2), θ, we would instead use the average angle, $\langle \theta \rangle = \langle \varphi_0 | \theta | \varphi_0 \rangle$, where $\varphi_0(\theta)$ is the ground vibrational wavefunction for the CO_2 bend. Returning to the CO_2 in the gas-phase thought experiment, the average angle is constant and equal to 180°. Thus, there would correctly be no contribution to CO_2 asymmetric stretch vibrational frequency. In contrast, the instantaneous average bend angle will fluctuate away from 180° in an IL because of asymmetric

solvation by the solvent. Of course, we do not have access to vibrational wavefunction for the CO_2 bend for the benchmark CO_2-$[C_4C_1im][PF_6]$ clusters, nor when we wanted to utilize the spectroscopic map to analyze an MD simulation. An additional approximation is necessary. If we were to regard the CO_2 bend as harmonic, then the average angle is given by the instantaneous distortion of the CO_2 geometry by the environment. For the benchmark clusters, the geometry distortion can be determined by optimizing the geometry of the CO_2 molecule using the classical MD force field and a conjugate gradient minimization while holding fixed both the center-of-mass of the CO_2, as well as the configuration of the IL solvent. The map is then used to calculate the vibrational frequency for the relaxed snapshot.

Figure 5b shows the distribution of CO_2 asymmetric stretch vibrational frequencies computed using the spectroscopic map for 1000 statistically independent snapshots collected from an MD simulation of flexible CO_2 in $[C_4C_1im][PF_6]$ where the CO_2 bend angle has been relaxed. On average, the relaxed bend angle is 178.4º, and the distribution of frequencies is nearly symmetric with a mean frequency of 2343.8 cm^{-1} and a standard deviation of 2.4 cm^{-1}. The mean frequency is in excellent agreement with experiment and differs by only 1.3 cm^{-1}. Note that this agreement implies that the spectroscopic map is able to accurately capture the solvatochromic shift of the CO_2 asymmetric stretch vibrational frequency from the gas-phase to the $[C_4C_1im][PF_6]$ IL. The width of the distribution is too narrow compared to the estimated width of the experimental distribution of 6.3 – 10.2 cm^{-1}. There are several possible sources for the discrepancy in the width of the distribution, including inaccuracies associated with the approximate perturbative approach for the effect of the bend on the asymmetric stretch frequency. However, the overall agreement with experiment is encouraging.

It is instructive to compare the distributions in Figures 5b (relaxed CO_2) and 5c (rigid CO_2). Both distributions are symmetric and they have nearly the same widths: 2.4 and 2.3 cm^{-1}, respectively. Thus, within the approximate perturbative approach, the bend has very little influence on the width of the distribution. The averages of the distributions differ more significantly: 2343.8 and 2346.5 cm^{-1}, respectively. The bend shifts the distribution to the red and into better agreement with experiment. Overall, the role of the bend is relatively minor resulting in a redshift of the distribution by 2.7 cm^{-1}. These results suggest several options for how the bend is treated when the map is applied in conjunction with MD simulations to understand the spectroscopy and spectral diffusion dynamics of CO_2 in the $[C_4C_1im][PF_6]$ IL in Paper III in this series. The simplest strategy is to hold the CO_2 rigid and to shift the calculated frequencies by 2.7 cm^{-1}. In essence, this would just account for the average effect of the CO_2 angle on the asymmetric stretch frequencies. A more computationally intensive strategy is a simulation with CO_2 flexible, but where the geometry of the CO_2 is optimized using the classical force field. The efficacy of these approaches will be evaluated in Paper III.

VI. Conclusions

In this paper we have developed and validated a spectroscopic map that is the foundation for a molecular interpretation of ultrafast vibrational spectroscopy of CO_2 in ionic liquids. In addition, we have established important insights into the solvatochromic shift of the CO_2 asymmetric stretch vibrational frequency in ILs. We analyzed the physical origin of the vibrational frequency shifts using SAPT energy decomposition schemes. Unlike other vibrational chromophores, electrostatics alone poorly predict the vibrational frequency. While the most

important contributor to the electrostatic part of the spectroscopic map is the field from the anion, both attractive dispersion interactions and repulsive charge overlap forces (Pauli repulsion) play additional important roles. Finally, while the CO_2 bend angle influences the asymmetric stretch frequency, we have shown that the geometry of the CO_2 molecule is only slightly perturbed by the IL, so regarding the CO_2 as rigid is generally sufficient to capture the structural relaxation of the IL relative to the CO_2.

Supporting Information

Details regarding the transition dipole moment integral calculations in Figure 3 are included in the Supporting Information. This material is available free of charge.

Acknowledgements

References

(1)   Karadas, F.; Atilhan, M.; Aparicio, S. Review on the Use of Ionic Liquids (ILs) as Alternative Fluids for CO_2 Capture and Natural Gas Sweetening. *Energy and Fuels* **2010**, *24* (11), 5817–5828.

(2)   Wishart, J. F. Energy Applications of Ionic Liquids. *Energy Environ. Sci.* **2009**, *2* (9), 956–961.

(3)   Armand, M.; Endres, F.; MacFarlane, D. R.; Ohno, H.; Scrosati, B. Ionic-Liquid Materials for the Electrochemical Challenges of the Future. *Nat. Mater.* **2009**, *8* (8), 621–629.

(4)   Patel, D. D.; Lee, J. M. Applications of Ionic Liquids. *Chem. Rec.* **2012**, *12* (3), 329–355.

(5)   Bara, J. E.; Camper, D. E.; Gin, D. L.; Noble, R. D. Room-Temperature Ionic Liquids and Composite Materials: Platform Technologies for CO_2 Capture. *Acc. Chem. Res.* **2010**, *43* (1), 152–159.

(6)   Crosthwaite, J. M.; Muldoon, M. J.; Dixon, J. K.; Anderson, J. L.; Brennecke, J. F. Phase Transition and Decomposition Temperatures, Heat Capacities and Viscosities of Pyridinium Ionic Liquids. *J. Chem. Thermodyn.* **2005**, *37* (6), 559–568.

(7)   Seki, S.; Kobayashi, T.; Kobayashi, Y.; Takei, K.; Miyashiro, H.; Hayamizu, K.; Tsuzuki, S.; Mitsugi, T.; Umebayashi, Y. Effects of Cation and Anion on Physical Properties of Room-Temperature Ionic Liquids. *J. Mol. Liq.* **2010**, *152* (1–3), 9–13.

(8)   Tokuda, H.; Hayamizu, K.; Ishii, K.; Susan, M. A. B. H.; Watanabe, M. Physicochemical Properties and Structures of Room Temperature Ionic Liquids. 2. Variation of Alkyl Chain Length in Imidazolium Cation. *J. Phys. Chem. B* **2005**, *109* (13), 6103–6110.

(9)   Anthony, J. L.; Maginn, E. J.; Brennecke, J. F. Solubilities and Thermodynamic Properties

of Gases in the Ionic Liquid 1-N-Butyl-3-Methylimidazolium Hexafluorophosphate. *J. Phys. Chem. B* **2002**, *106* (29), 7315–7320.

(10) Seo, S.; Quiroz-Guzman, M.; Desilva, M. A.; Lee, T. B.; Huang, Y.; Goodrich, B. F.; Schneider, W. F.; Brennecke, J. F. Chemically Tunable Ionic Liquids with Aprotic Heterocyclic Anion (AHA) for CO_2 Capture. *J. Phys. Chem. B* **2014**, *118* (21), 5740–5751.

(11) Shiflett, M. B.; Yokozeki, A. Solubilities and Diffusivities of Carbon Dioxide in Ionic Liquids: [bmim][PF_6] and [bmim][BF_4]. *Ind. Eng. Chem. Res.* **2005**, *44* (12), 4453–4464.

(12) Gurkan, B. E.; De La Fuente, J. C.; Mindrup, E. M.; Ficke, L. E.; Goodrich, B. F.; Price, E. A.; Schneider, W. F.; Brennecke, J. F. Equimolar CO_2 Absorption by Anion-Functionalized Ionic Liquids. *J. Am. Chem. Soc.* **2010**, *132* (7), 2116–2117.

(13) Cadena, C.; Anthony, J. L.; Shah, J. K.; Morrow, T. I.; Brennecke, J. F.; Maginn, E. J. Why Is CO_2 so Soluble in Imidazolium-Based Ionic Liquids? *J. Am. Chem. Soc.* **2004**, *126* (16), 5300–5308.

(14) Tamimi, A.; Fayer, M. D. Ionic Liquid Dynamics Measured with 2D IR and IR Pump–Probe Experiments on a Linear Anion and the Influence of Potassium Cations. *J. Phys. Chem. B* **2016**, *120* (26), 5842–5854.

(15) Ren, Z.; Ivanova, A. S.; Couchot-Vore, D.; Garrett-Roe, S. Ultrafast Structure and Dynamics in Ionic Liquids: 2D-IR Spectroscopy Probes the Molecular Origin of Viscosity. *J. Phys. Chem. Lett.* **2014**, *5* (9), 1541–1546.

(16) Hamm, P.; Zanni, M. *Concepts and Methods of 2D Infrared Spectroscopy*; Cambridge University Press, 2015.

(17) Khalil, M.; Demirdöven, N.; Tokmakoff, A. Coherent 2D IR Spectroscopy: Molecular

Structure and Dynamics in Solution. *J. Phys. Chem. A* **2003**, *107* (27), 5258–5279.

(18)   Levinson, N. M.; Bolte, E. E.; Miller, C. S.; Corcelli, S. A.; Boxer, S. G. Phosphate

Vibrations Probe Local Electric Fields and Hydration in Biomolecules. *J. Am. Chem. Soc.*

2011, *133* (34), 13236–13239.

(19)   Choi, J. H.; Cho, M. Vibrational Solvatochromism and Electrochromism of Infrared Probe

Molecules Containing C≡O, C≡N, C=O, or C-F Vibrational Chromophore. *J. Chem. Phys.*

2011, *134* (15), 154513.

(20)   Choi, J. H.; Oh, K. I.; Lee, H.; Lee, C.; Cho, M. Nitrile and Thiocyanate IR Probes:

Quantum Chemistry Calculation Studies and Multivariate Least-Square Fitting Analysis.

J. Chem. Phys. **2008**, *128* (13), 134506.

(21)   Lee, K. K.; Park, K. H.; Kwon, D.; Choi, J. H.; Son, H.; Park, S.; Cho, M. Ion-Pairing

Dynamics of Li^+ and SCN^- in Dimethylformamide Solution: Chemical Exchange Two-

Dimensional Infrared Spectroscopy. *J. Chem. Phys.* **2011**, *134* (6), 64506.

(22)   Steinel, T.; Asbury, J. B.; Corcelli, S. A.; Lawrence, C. P.; Skinner, J. L.; Fayer, M. D.

Water Dynamics: Dependence on Local Structure Probed with Vibrational Echo

Correlation Spectroscopy. *Chem. Phys. Lett.* **2004**, *386* (4–6), 295–300.

(23)   Brinzer, T.; Berquist, E. J.; Ren, Z.; Dutta, S.; Johnson, C. A.; Krisher, C. S.; Lambrecht,

D. S.; Garrett-Roe, S. Ultrafast Vibrational Spectroscopy (2D-IR) of CO_2 in Ionic Liquids:

Carbon Capture from Carbon Dioxide's Point of View. *J. Chem. Phys.* **2015**, *142* (21),

212425.

(24)   Giammanco, C. H.; Kramer, P. L.; Yamada, S. A.; Nishida, J.; Tamimi, A.; Fayer, M. D.

Carbon Dioxide in an Ionic Liquid: Structural and Rotational Dynamics. *J. Chem. Phys.*

2016, *144* (10), 104506.

(25) Giammanco, C. H.; Kramer, P. L.; Yamada, S. A.; Nishida, J.; Tamimi, A.; Fayer, M. D. Coupling of Carbon Dioxide Stretch and Bend Vibrations Reveals Thermal Population Dynamics in an Ionic Liquid. *J. Phys. Chem. B* **2016**, *120* (3), 549–556.

(26) Asbury, J. B.; Steinel, T.; Kwak, K.; Corcelli, S. A.; Lawrence, C. P.; Skinner, J. L.; Fayer, M. D. Dynamics of Water Probed with Vibrational Echo Correlation Spectroscopy. *J. Chem. Phys.* **2004**, *121* (24), 12431–12446.

(27) Asbury, J. B.; Steinel, T.; Stromberg, C.; Corcelli, S. A.; Lawrence, C. P.; Skinner, J. L.; Fayer, M. D. Water Dynamics: Vibrational Echo Correlation Spectroscopy and Comparison to Molecular Dynamics Simulations. *J. Phys. Chem. A* **2004**, *108* (7), 1107–1119.

(28) Bakker, H. J.; Skinner, J. L. Vibrational Spectroscopy as a Probe of Structure and Dynamics in Liquid Water. *Chem. Rev.* **2010**, *110* (3), 1498–1517.

(29) Fecko, C. J.; Eaves, J. D.; Loparo, J. J.; Tokmakoff, A.; Geissler, P. L. Ultrafast Hydrogen-Bond Dynamics in the Infrared Spectroscopy of Water. *Science* **2003**, *301* (5640), 1698–1702.

(30) Eaves, J. D.; Loparo, J. J.; Fecko, C. J.; Roberts, S. T.; Tokmakoff, A.; Geissler, P. L. Hydrogen Bonds in Liquid Water Are Broken Only Fleetingly. *Proc. Natl. Acad. Sci. U. S. A.* **2005**, *102* (37), 13019–13022.

(31) Gruenbaum, S. M.; Tainter, C. J.; Shi, L.; Ni, Y.; Skinner, J. L. Robustness of Frequency, Transition Dipole, and Coupling Maps for Water Vibrational Spectroscopy. *J. Chem. Theory Comput.* **2013**, *9* (7), 3109–3117.

(32) Jansen, T. L. C.; Auer, B. M.; Yang, M.; Skinner, J. L. Two-Dimensional Infrared Spectroscopy and Ultrafast Anisotropy Decay of Water. *J. Chem. Phys. J. Chem. Phys. J.*

Chem. Phys. J. Chem. Phys. J. Chem. Phys. J. Chem. Phys **2010**, *1321* (10), 224503–164301.

(33)   Loparo, J. J.; Roberts, S. T.; Tokmakoff, A. Multidimensional Infrared Spectroscopy of Water. I. Vibrational Dynamics in Two-Dimensional IR Line Shapes. *J. Chem. Phys.* **2006**, *125* (19), 194521.

(34)   Loparo, J. J.; Roberts, S. T.; Tokmakoff, A. Multidimensional Infrared Spectroscopy of Water. II. Hydrogen Bond Switching Dynamics. *J. Chem. Phys.* **2006**, *125* (19), 194522.

(35)   Nibbering, E. T. J.; Elsaesser, T. Ultrafast Vibrational Dynamics of Hydrogen Bonds in the Condensed Phase. *Chem. Rev.* **2004**, *104* (4), 1887–1914.

(36)   Nicodemus, R. A.; Corcelli, S. A.; Skinner, J. L.; Tokmakoff, A. Collective Hydrogen Bond Reorganization in Water Studied with Temperature-Dependent Ultrafast Infrared Spectroscopy. *J. Phys. Chem. B* **2011**, *115* (18), 5604–5616.

(37)   Nicodemus, R. A.; Ramasesha, K.; Roberts, S. T.; Tokmakoff, A. Hydrogen Bond Rearrangements in Water Probed with Temperature-Dependent 2D IR. *J. Phys. Chem. Lett.* **2010**, *1* (7), 1068–1072.

(38)   Ramasesha, K.; Roberts, S. T.; Nicodemus, R. A.; Mandal, A.; Tokmakoff, A. Ultrafast 2D IR Anisotropy of Water Reveals Reorientation during Hydrogen-Bond Switching. *J. Chem. Phys.* **2011**, *135* (5), 12457–54509.

(39)   Roberts, S. T.; Ramasesha, K.; Tokmakoff, A. Structural Rearrangements in Water Viewed through Two-Dimensional Infrared Spectroscopy. *Acc. Chem. Res.* **2009**, *42* (9), 1239–1249.

(40)   Auer, B.; Kumar, R.; Schmidt, J. R.; Skinner, J. L. Hydrogen Bonding and Raman, IR, and 2D-IR Spectroscopy of Dilute HOD in Liquid D_2O. *Proc. Natl. Acad. Sci. USA* **2007**,

104 (36), 14215–14220.

(41)   Auer, B. M.; Skinner, J. L. IR and Raman Spectra of Liquid Water: Theory and

Interpretation. *J. Chem. Phys.* **2008**, *128* (22), 224511.

(42)   Corcelli, S. A.; Lawrence, C. P.; Skinner, J. L. Combined Electronic Structure/molecular

Dynamics Approach for Ultrafast Infrared Spectroscopy of Dilute HOD in Liquid H_2O

and D_2O. *J. Chem. Phys.* **2004**, *120* (17), 8107–8117.

(43)   Hayashi, T.; la Cour Jansen, T.; Zhuang, W.; Mukamel, S. Collective Solvent Coordinates

for the Infrared Spectrum of HOD in D_2O Based on an *Ab Initio* Electrostatic Map. *J.

Phys. Chem. A* **2005**, *109* (1), 64–82.

(44)   Jansen, T. L. C.; Cringus, D.; Pshenichnikov, M. S. Dissimilar Dynamics of Coupled

Water Vibrations. *J. Phys. Chem. A* **2009**, *113* (22), 6260–6265.

(45)   Li, F.; Skinner, J. L. Infrared and Raman Line Shapes for Ice I_h. II. H_2O and D_2O. *J.

Chem. Phys.* **2010**, *133* (24), 244504–244504.

(46)   Lin, Y. S.; Li, G. De; Mao, S. P.; Chai, J. Da. Long-Range Corrected Hybrid Density

Functionals with Improved Dispersion Corrections. *J. Chem. Theory Comput.* **2013**, *9* (1),

263–272.

(47)   Lin, Y. S.; Auer, B. M.; Skinner, J. L. Water Structure, Dynamics, and Vibrational

Spectroscopy in Sodium Bromide Solutions. *J. Chem. Phys.* **2009**, *131* (14), 144511.

(48)   Paarmann, A.; Hayashi, T.; Mukamel, S.; Miller, R. J. D. Nonlinear Response of

Vibrational Excitons: Simulating the Two-Dimensional Infrared Spectrum of Liquid

Water. *J. Chem. Phys.* **2009**, *130* (20), 204110.

(49)   Pieniazek, P. A.; Lin, Y.-S.; Chowdhary, J.; Ladanyi, B. M.; Skinner, J. L. Vibrational

Spectroscopy and Dynamics of Water Confined inside Reverse Micelles. *J. Phys. Chem. B*

2009, *113* (45), 15017–15028.

(50) Shi, L.; Gruenbaum, S. M.; Skinner, J. L. Interpretation of IR and Raman Line Shapes for H_2O and D_2O Ice I_h. *J. Phys. Chem. B* **2012**, *116* (47), 13821–13830.

(51) Skinner, J.; Auer, B.; Lin, Y. Vibrational Line Shapes, Spectral Diffusion, and Hydrogen Bonding in Liquid Water. *Adv. Chem. Phys.* **2009**, *142*, 59.

(52) Tainter, C. J.; Skinner, J. L. The Water Hexamer: Three-Body Interactions, Structures, Energetics, and OH-Stretch Spectroscopy at Finite Temperature. *J. Chem. Phys.* **2012**, *137* (10), 2351–104304.

(53) Yang, M.; Skinner, J. L. Time-Averaging Approximation in the Interaction Picture: Absorption Line Shapes for Coupled Chromophores with Application to Liquid Water. *J. Chem. Phys.* **2011**, *135* (15), 154114.

(54) Laage, D.; Hynes, J. T. Do More Strongly Hydrogen-Bonded Water Molecules Reorient More Slowly ? *Chem. Phys. Lett.* **2006**, *433* (1–3), 80–85.

(55) Laage, D. A Molecular Jump Mechanism of Water Reorientation. *Science* **2006**, *311* (5762), 832–835.

(56) Laage, D.; Hynes, J. T. On the Molecular Mechanism of Water Reorientation. *J. Phys. Chem. B* **2008**, *112* (45), 14230–14242.

(57) Laage, D.; Stirnemann, G.; Hynes, J. T. Water Jump Reorientation and Ultrafast Vibrational Spectroscopy. *J. Photochem. Photobiol. A Chem.* **2012**, *234*, 75–82.

(58) Laage, D.; Stirnemann, G.; Sterpone, F.; Hynes, J. T. Water Jump Reorientation: From Theoretical Prediction to Experimental Observation. *Acc. Chem. Res.* **2012**, *45* (1), 53–62.

(59) Smith, J. D.; Cappa, C. D.; Wilson, K. R.; Cohen, R. C.; Geissler, P. L.; Saykally, R. J. Unified Description of Temperature-Dependent Hydrogen-Bond Rearrangements in

Liquid Water. *Proc. Natl. Acad. Sci.* **2005**, *102* (40), 14171–14174.

(60)   Li, S.; Schmidt, J. R.; Corcelli, S. A.; Lawrence, C. P.; Skinner, J. L. Approaches for the Calculation of Vibrational Frequencies in Liquids: Comparison to Benchmarks for Azide/water Clusters. *J. Chem. Phys.* **2006**, *124* (20), 204110.

(61)   Terranova, Z. L.; Corcelli, S. A. Molecular Dynamics Investigation of the Vibrational Spectroscopy of Isolated Water in an Ionic Liquid. *J. Phys. Chem. B* **2014**, *118* (28), 8264–8272.

(62)   Oh, K. I.; Choi, J. H.; Lee, J. H.; Han, J. B.; Lee, H.; Cho, M. Nitrile and Thiocyanate IR Probes: Molecular Dynamics Simulation Studies. *J. Chem. Phys.* **2008**, *128* (15), 154504.

(63)   Corcelli, S. A.; Skinner, J. L. Infrared and Raman Line Shapes of Dilute HOD in Liquid H_2O and D_2O from 10 to 90°C. *J. Phys. Chem. A* **2005**, *109* (28), 6154–6165.

(64)   Schmidt, J. R.; Corcelli, S. A.; Skinner, J. L. Pronounced Non-Condon Effects in the Ultrafast Infrared Spectroscopy of Water. *J. Chem. Phys.* **2005**, *123* (4), 044513.

(65)   Błasiak, B.; Lee, H.; Cho, M. Vibrational Solvatochromism: Towards Systematic Approach to Modeling Solvation Phenomena. *J. Chem. Phys.* **2013**, *139* (4), 044111.

(66)   Błasiak, B.; Cho, M. Vibrational Solvatochromism. II. A First-Principle Theory of Solvation-Induced Vibrational Frequency Shift Based on Effective Fragment Potential Method. *J. Chem. Phys.* **2014**, *140* (16), 164107.

(67)   Berquist, E. J.; Daly, C. A. J.; Brinzer, T.; Bullard, K. K.; Campbell, Z. M.; Corcelli, S. A.; Garrett-Roe, S.; Lambrecht, D. S. Modeling Carbon Dioxide Vibrational Frequencies in Ionic Liquids I. *Ab Initio* Calculations. *J. Phys. Chem.* (submitted).

(68)   Błasiak, B.; Cho, M. Vibrational Solvatochromism. III. Rigorous Treatment of the Dispersion Interaction Contribution. *J. Chem. Phys.* **2015**, *143* (16), 164111.

(69)   Jeziorski, B.; Moszynski, R.; Szalewicz, K. Perturbation Theory Approach to Intermolecular Potential Energy Surfaces of van Der Waals Complexes. *Chem. Rev.* **1994**, *94* (7), 1887–1930.

(70)   Hohenstein, E. G.; Sherrill, C. D. Density Fitting and Cholesky Decomposition Approximations in Symmetry-Adapted Perturbation Theory: Implementation and Application to Probe the Nature of π-π Interactions in Linear Systems. *J. Chem. Phys.* **2010**, *132* (18).

(71)   Hohenstein, E. G.; Parrish, R. M.; Sherrill, C. D.; Turney, J. M.; Schaefer, H. F. Large-Scale Symmetry-Adapted Perturbation Theory Computations via Density Fitting and Laplace Transformation Techniques: Investigating the Fundamental Forces of DNA-Intercalator Interactions. *J. Chem. Phys.* **2011**, *135* (17) 184111.

(72)   Plimpton, S. Fast Parallel Algorithms for Short-Range Molecular Dynamics. *J. Comput. Phys.* **1995**, *117* (1), 1–19.

(73)   Andreussi, O.; Marzari, N. Transport Properties of Room-Temperature Ionic Liquids from Classical Molecular Dynamics. *J. Chem. Phys.* **2012**, *137* (4), 44508.

(74)   Forester, T. R.; Smith, W. SHAKE, Rattle, and Roll: Efficient Constraint Algorithms for Linked Rigid Bodies. *J. Comput. Chem.* **1998**, *19* (1), 102–111.

(75)   Ryckaert, J. P.; Ciccotti, G.; Berendsen, H. J. C. Numerical Integration of the Cartesian Equations of Motion of a System with Constraints: Molecular Dynamics of N-Alkanes. *J. Comput. Phys.* **1977**, *23* (3), 327–341.

(76)   Sprenger, K. G.; Jaeger, V. W.; Pfaendtner, J. The General AMBER Force Field (GAFF) Can Accurately Predict Thermodynamic and Transport Properties of Many Ionic Liquids. *J. Phys. Chem. B* **2015**, *119* (18), 5882–5895.

(77)   Wang, J.; Wolf, R. Development and Testing of a General Amber Force Field. *J. Comput. Chem.* **2004**, *25* (25), 1157–1174.

(78)   Singh, U. C.; Kollman, P. A. A Combined *Ab Initio* Quantum Mechanical and Molecular Mechanical Method for Carrying out Simulations on Complex Molecular Systems: Applications to the $CH_3Cl + Cl^-$ Exchange Reaction and Gas Phase Protonation of Polyethers. *J. Comput. Chem.* **1986**, *7* (6), 718.

(79)   Liu, Z.; Huang, S.; Wang, W. A Refined Force Field for Molecular Simulation of Imidazolium-Based Ionic Liquids. *J. Phys. Chem. B* **2004**, *108* (34), 12978–12989.

(80)   Chaban, V. V; Voroshylova, I. V; Kalugin, O. N. A New Force Field Model for the Simulation of Transport Properties of Imidazolium-Based Ionic Liquids. *Phys. Chem. Chem. Phys.* **2011**, *13* (17), 7910–7920.

(81)   Schröder, C. Comparing Reduced Partial Charge Models with Polarizable Simulations of Ionic Liquids. *Phys. Chem. Chem. Phys.* **2012**, *14* (9), 3089–3102.

(82)   Potoff, J. J.; Siepmann, J. I. Vapor–liquid Equilibria of Mixtures Containing Alkanes, Carbon Dioxide, and Nitrogen. *AIChE J.* **2001**, *47* (7), 1676–1682.

(83)   Perez-Blanco, M. E.; Maginn, E. J. Molecular Dynamics Simulations of CO_2 at an Ionic Liquid Interface: Adsorption, Ordering, and Interfacial Crossing. *J. Phys. Chem. B* **2010**, *114* (36), 11827–11837.

(84)   Darden, T.; York, D.; Pedersen, L. Particle Mesh Ewald: An N· log(N) Method for Ewald Sums in Large Systems. *J. Chem. Phys.* **1993**, *98* (12), 10089.

(85)   Małolepsza, E.; Straub, J. E. Empirical Maps for the Calculation of Amide I Vibrational Spectra of Proteins from Classical Molecular Dynamics Simulations. *J. Phys. Chem. B* **2014**, *118* (28), 7848–7855.

(86) Fennell, C. J.; Gezelter, J. D. Is the Ewald Summation Still Necessary? Pairwise Alternatives to the Accepted Standard for Long-Range Electrostatics. *J. Chem. Phys.* **2006**, *124* (23), 234104.

(87) Loparo, J. J.; Roberts, S. T.; Nicodemus, R. A.; Tokmakoff, A. Variation of the Transition Dipole Moment across the OH Stretching Band of Water. *Chem. Phys.* **2007**, *341* (1–3), 218–229.

(88) Miller, C. S.; Ploetz, E. A.; Cremeens, M. E.; Corcelli, S. A. Carbon-Deuterium Vibrational Probes of Peptide Conformation: Alanine Dipeptide and Glycine Dipeptide. *J. Chem. Phys.* **2009**, *130* (12).

(89) Aki, S. N. V. K.; Mellein, B. R.; Saurer, E. M.; Brennecke, J. F. High-Pressure Phase Behavior of Carbon Dioxide with Imidazolium-Based Ionic Liquids. *J. Phys. Chem. B* **2004**, *108*, 20355–20365.

(90) Anthony, J. L.; Anderson, J. L.; Maginn, E. J.; Brennecke, J. F. Anion Effects on Gas Solubility in Ionic Liquids. *J. Phys. Chem. B* **2005**, *109*, 6366–6374.

(91) Muldoon, M. J.; Aki, S. N. V. K.; Anderson, J. L.; Dixon, J. K.; Brennecke, J. F. Improving Carbon Dioxide Solubility in Ionic Liquids. *J. Phys. Chem. B* **2007**, *111* (30), 9001–9009.

(92) Hou, Y.; Baltus, R. E. Experimental Measurement of the Solubility and Diffusivity of CO_2 in Room-Temperature Ionic Liquids Using a Transient Thin-Liquid-Film Method. *Ind. Eng. Chem. Res.* **2007**, *46* (24), 8166–8175.

(93) Ramdin, M.; De Loos, T. W.; Vlugt, T. J. H. State-of-the-Art of CO_2 Capture with Ionic Liquids. *Ind. Eng. Chem. Res.* **2012**, *51* (24), 8149–8177.

(94) Stenger, J.; Madsen, D.; Hamm, P.; Nibbering, E. T. J.; Elsaesser, T. Ultrafast Vibrational

Dephasing of Liquid Water. *Phys. Rev. Lett.* **2001**, *87* (2), 27401.

(95)   Rosenthal, S. J.; Xie, X.; Du, M.; Fleming, G. R. Femtosecond Solvation Dynamics in

Acetonitrile: Observation of the Inertial Contribution to the Solvent Response. *J. Chem.*

Phys. **1991**, *95* (6), 4715.

Table 1. Parameters of the spectroscopic map for the CO_2 asymmetric stretch frequency in $[C_4C_1im][PF_6]$. This map predicts the CO_2 with a regression coefficient $R = 0.94$ and a root mean square error of 2.7 cm^{-1}. The average shift, $\langle\Delta\omega\rangle$, and standard deviation, $\sigma(\Delta\omega)$, are reported for each term in the map.

		$\langle\Delta\omega\rangle$ (cm^{-1})	$\sigma(\Delta\omega)$ (cm^{-1})
ω_g	2349.1 cm^{-1}	0.0	0.0
a	−1160.9 cm^{-1}	−6.6	7.0
b_1	64.4 cm^{-1} au^{-1}	−0.1	0.4
b_2	93.2 cm^{-1} au^{-1}	−1.8	0.7
c_1	4.70 cm^{-1} kcal^{-1} mol	−9.5	2.0
c_2	−3.55 cm^{-1} kcal^{-1} mol	7.3	2.1

Table 2. Decomposition of the average LJ contribution to the spectroscopic map for the CO_2 asymmetric stretch frequency in [C$_4$C$_1$im][PF$_6$] into attractive and repulsive components.

LJ Component	Site	$\langle \Delta\omega \rangle$ (cm^{-1})
	O	–21.7
Attractive	C	14.8
	Sum	–6.9
	O	12.3
Repulsive	C	–7.4
	Sum	4.9
	O	–9.4
Total	C	7.3
	Sum	–2.1

Figure 1. Relationship between the CO_2 asymmetric stretch vibrational frequency and the OCO angle, θ_{OCO}, for CO_2 in the gas-phase (green circles) and in the $[C_4C_1im][PF_6]$ IL (black circles). The gas-phase data are perfectly correlated with $1 + \cos(\theta_{OCO})$. The vibrational frequencies for CO_2 in the $[C_4C_1im][PF_6]$ solvent also show this relationship, but additional solvation effects on the frequency are also present.
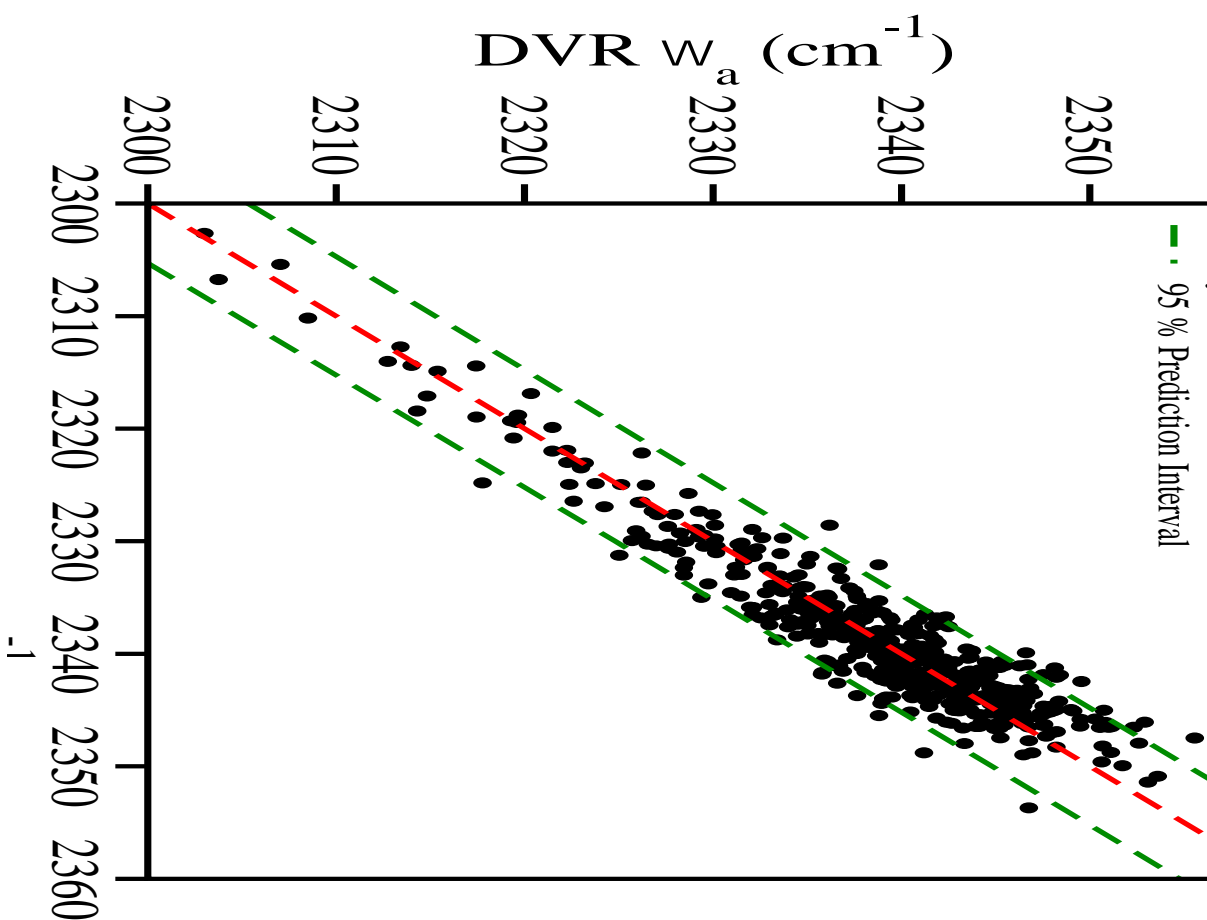
Figure 2. Relationship between CO_2 asymmetric stretch frequencies in the $[C_4C_1im][PF_6]$ IL calculated using the DVR method and those calculated using the spectroscopic map for the 500 test set clusters (black circles). The red line represents a perfect correlation and the 95% prediction interval is indicated with green lines. The spectroscopic map has a regression coefficient of R = 0.94 and a root means squared error of 2.7 cm^{-1}.
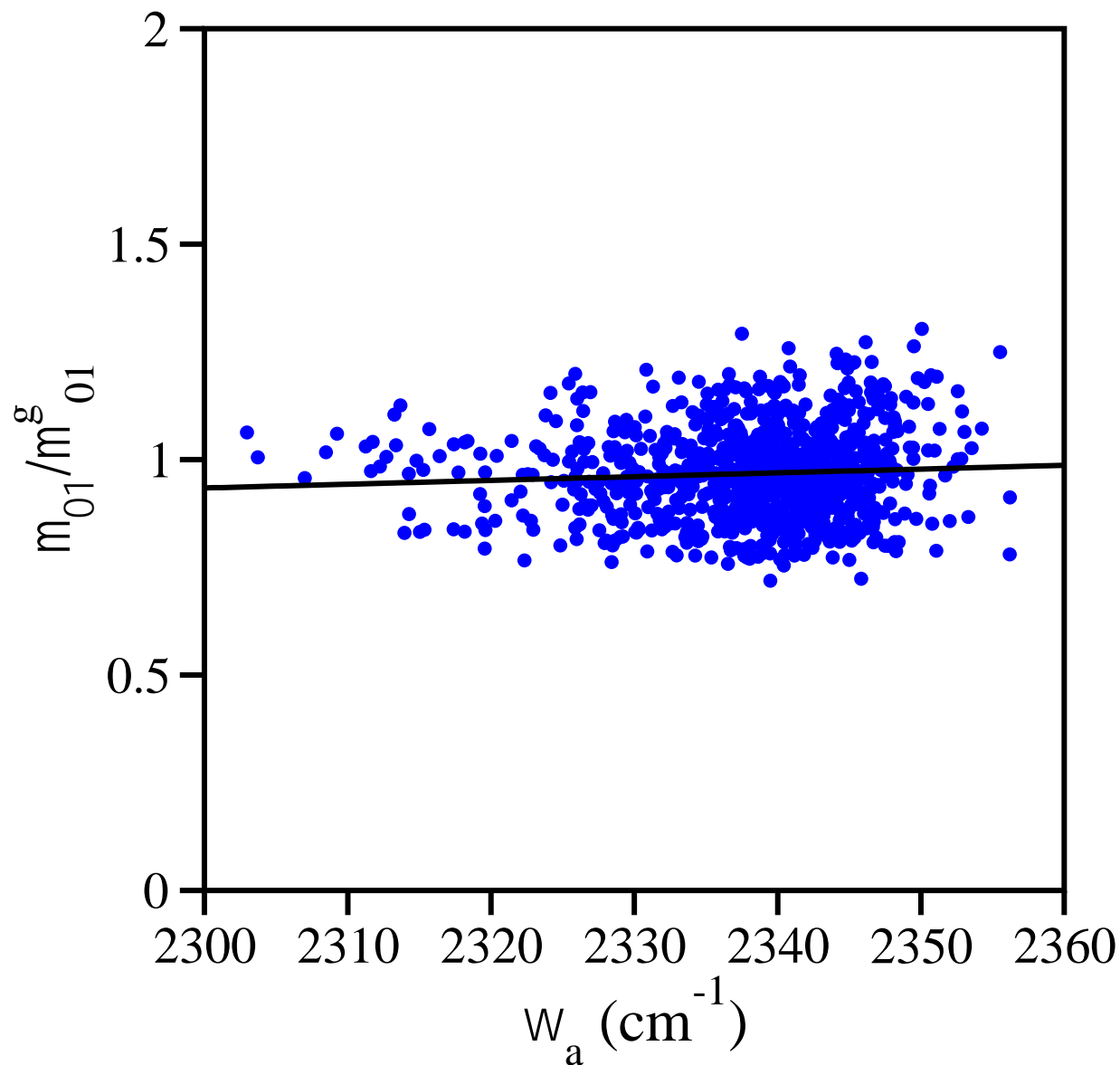
Figure 3. Transition dipole moment integral, μ_{01}, of the asymmetric stretch of CO_2 in 1000 CO_2-[C$_4$C$_1$im][PF$_6$] clusters versus the asymmetric stretch vibrational frequency, ω_a, where μ_{01}^g is the transition dipole moment integral of the asymmetric stretch of CO_2 in the gas-phase (blue circles). A linear fit of the data (black line) has a slope close to zero indicating that the Condon approximation is reasonable for the asymmetric stretch of CO_2 in the [C$_4$C$_1$im][PF$_6$] IL.

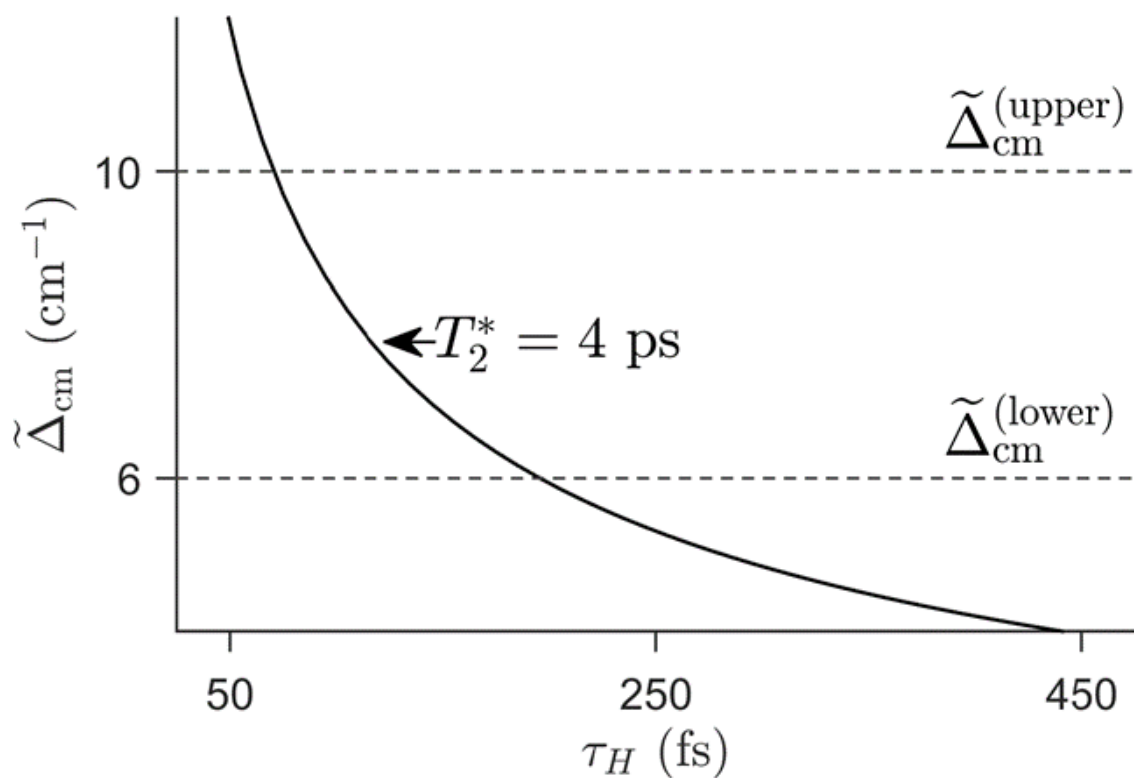**Figure 4.** Homogeneous instantaneous linewidth as a function of correlation time for fast motions, with $T_2^* = 4$ ps, with upper and lower bounds estimated for $\tilde{\Delta}_H$. The upper bound, based on an estimated fastest allowed inertial response timescale, and the lower bound, based on a threshold value of $\Delta_H\tau_H$, are indicated by dashed horizontal lines. The resulting instantaneous frequency range for homogeneous motions is between 6 and 10 cm^{-1}.
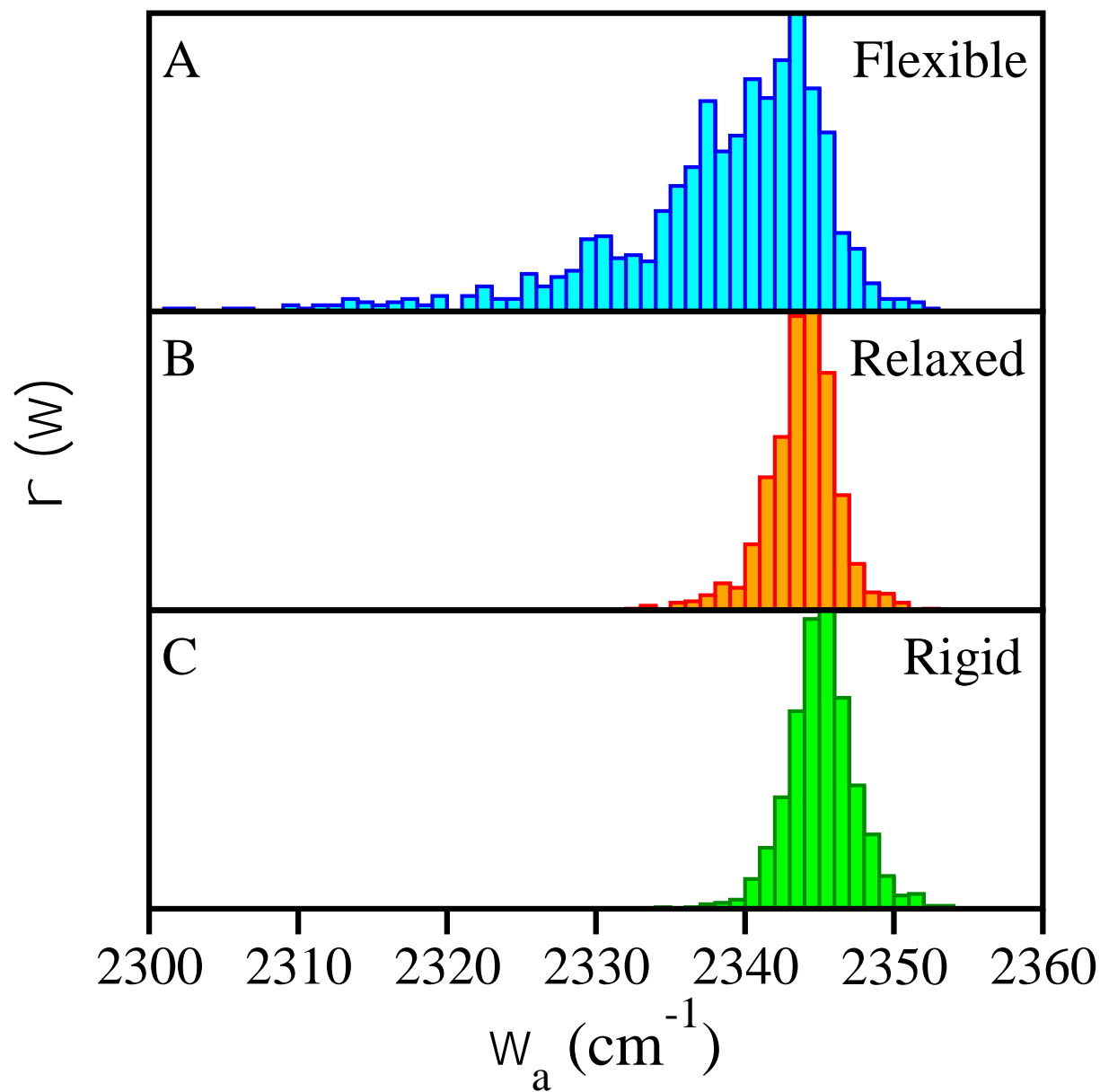
Figure 5. Histograms of the CO_2 asymmetric stretch vibrational frequency, ω_a, for 1000 CO_2-$[C_4C_1im][PF_6]$ clusters. (a) Clusters extracted from an MD simulation of flexible CO_2 in the $[C_4C_1im][PF_6]$ IL. (b) Clusters extracted from an MD simulation of flexible CO_2 in the $[C_4C_1im][PF_6]$ IL, but where the CO_2 geometry is relaxed. (c) Clusters extracted from an MD simulation of rigid CO_2 in the $[C_4C_1im][PF_6]$ IL.